Numerical simulation of growth of an atherosclerotic lesion with a moving boundary

Jens P. Eberhard* Peter Frolkovič*

May 22, 2006

Abstract

We consider a mathematical model of the formation of an atherosclerotic lesion that is based on a simplification of Russell Ross paradigm of atherosclerosis as a chronic inflammatory response. Atherosclerosis is characterized by the accumulation of lipid-laden cells in the arterial wall that can result in lesions within the artery. Such lesions can cause an occlusion of the artery resulting in heart attack.

The presented mathematical model describes, among others, a response of immune and smooth muscle cells to biochemical signals of chemoattractants and a build up of debris. It results in a coupled system of four nonlinear reaction-convection-diffusion equations including a free inner boundary that is permitted to move due to an additional evolution equation. We perform a numerical study of the problem using fully implicit finite volume discretization methods. The moving boundary is described implicitly using an evolution of a level set function. In such a way, a grid used in numerical simulation can remain fixed during the whole computations.

In this report, we present preliminary results that demonstrates that our numerical model captures certain observed features such as the localization of immune cells, the build-up of debris, the isolation of a lesion by smooth muscle cells, and an occlusion of the artery.

1 Introduction

In this report we deal with a mathematical model of atherosclerotic lesion formation including an intrusion into the lumen that was introduced in [7]. The problem is stated there in terms of a coupled system of nonlinear parabolic partial differential equations on a domain with a moving boundary. For numerical simulation of this model problem we propose here a finite volume discretization method combined with a level set formulation.

In the presented mathematical model of atherosclerosis, the focus lies on physical and chemical aspects of the disease. In particular, the model accounts for the process by which immune response cells travel into the arterial wall from the lumen in response to chemical signals secreted by a developing atherosclerotic lesion. In this process, some immune cells become corrupted as they take on lipid molecules. While a healthy macrophage can aid in the elimination of foreign bodies from the tissue, a lipid laden macrophage is incapable of performing this task and becomes part of the build up of debris forming a lesion. More immune cells are then summoned by chemical signals and an inflammatory process results. The chemoattractants can also invoke the chemotaxis of smooth muscle cells (SMCs), recruited primarily from the medial layer of the arterial wall, which layer over the lesion core to form a cap.

To describe this process, a mathematical model was introduced in [8, 7], where three generalized cellular species and three generalized chemical species elemental to the process were identified. We use here a simplified version of this model, see [8, 7], using assumptions that the concentrations of

*Simulation in Technology, University of Heidelberg, Im Neuenheimer Feld 368, D-69120 Heidelberg, Germany (eberhard@uni-hd.de)

native and oxidized low-density lipoproteins are fixed and high enough to coincide with a diseased state.

We follow the notation given in [8, 7]. The following three generalized cellular species and one generalized chemical specie are considered:

- Immune cells n_1 (number density). These are primarily macrophages, T-lymphocytes, and other immune response cells.
- Smooth muscle cells n_2 (number density). These cells also include any cells that are inherent in the production of the extra cellular matrix.
- Debris n_3 (number density). Debris is defined as dead cells, apoptic cells and foam cells.
- Chemoattractant c_1 (concentration). We make no distinction between various types of chemoattractants, i.e., c_1 refers to any chemical which induces positive chemotaxis.

Following [7] the system of equations reads

$$\frac{\partial n_1}{\partial t} = \mu_1 \Delta n_1 - \chi_{11}^0 \nabla \cdot \left(\frac{n_1}{c_1} \nabla c_1 \right) - d_1 n_1 n_3 \tag{1}$$

$$\frac{\partial n_2}{\partial t} = \mu_2 \Delta n_2 - \chi_{21}^0 \nabla \cdot \left(\frac{n_2}{c_1} \nabla c_1 \right) + \delta \nabla \cdot \left(\frac{n_2}{n_3} \nabla n_3 \right) - d_2 n_2 n_3 \tag{2}$$

$$\frac{\partial n_3}{\partial t} = \mu_3 \Delta n_3 + d_1 n_1 n_3 + d_2 n_2 n_3 \tag{3}$$

$$\frac{\partial c_1}{\partial t} = \nu_1 \Delta c_1 - \alpha_1 n_1 c_1 - \alpha_2 n_2 c_1 + \gamma n_3 \,. \tag{4}$$

Considering this system of partial differential equations on an annular fixed domain in R^2, one can impose the following initial and boundary conditions. For $x \in \Omega$

$$n_1(0,x) = 0 \qquad n_2(0,x) = 0 \tag{5}$$

$$n_3(0,x) = \epsilon_3 \exp(-Q_3 |x_0 - x|^2) \qquad c_1(0,x) = c_1^0 \,, \tag{6}$$

for the inner boundary, $x \in \Gamma_0$,

$$\frac{\partial n_1}{\partial \eta} = -\frac{1}{2} \hat{\beta}_0 (c_1 - c_1^*) \qquad \frac{\partial n_2}{\partial \eta} = 0 \tag{7}$$

$$\frac{\partial n_3}{\partial \eta} = 0 \qquad \frac{\partial c_1}{\partial \eta} = 0 \,, \tag{8}$$

and for the outer boundary, $x \in \Gamma_1$,

$$\frac{\partial n_1}{\partial \eta} = 0 \qquad \frac{\partial n_2}{\partial \eta} = -\hat{\beta}_1 (c_1 - c_1^{**}) \tag{9}$$

$$\frac{\partial n_3}{\partial \eta} = 0 \qquad \frac{\partial c_1}{\partial \eta} = 0 \tag{10}$$

where $\hat{\beta}_j(x) = \beta_j H(x) x^2 / (\alpha_j + x^2)$ and $H(x)$ denotes the Heaviside function. β_j, α_j are positive constants.

We remark that the nonzero flux condition for n_1 at the inner boundary shows that immune cells enter into the intima at a rate $\hat{\beta}_0(c_1 - c_1^*)$ provided that the amount of chemoattractant is above a threshold value c_1^*. Since the smooth muscle cells migrate from the media there is an analogous condition on these cells at the outer boundary. We assume a small uniform distribution of chemoattractant initially. The domain is "seeded" with a small amount of debris at the arbitrarily chosen point x_0. All other species are assumed to be absent initially. Furthermore, d_i, $i = 1, 2$, denote positive constants, and the diffusion coefficients μ_i, $i = 1, 2, 3$, and ν_1 are constant. χ_{ij}^0 denote the various chemotactic sensitivity values.

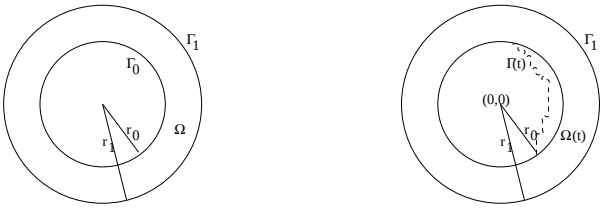

Figure 1: Sketch of the annulus and the domain. Left: The fixed domain and the active part at the initialization. Right: The annulus showing the moving inner boundary of the active part of the domain.

2 Free boundary problem

Instead of a fixed inner circle boundary Γ_0 we consider in the following a freely moving inner boundary which is denoted by $\Gamma(t)$. The domain is therefore time-dependent and is denoted by $\Omega(t)$. The outer boundary Γ_1 of $\Omega(t)$ is still a fixed circle of radius r_1. The inner boundary is initially a circle, $\Gamma_0 = \Gamma(0)$, with radius $r_0 < r_1$. The system must be supplemented with an equation prescribing the evolution of the inner boundary $\Gamma(t)$ as it responds to the growing lesion.

To reflect the moving boundary in the model problem, it has to be reformulated, as shown in [7], to incorporate the native tissue. To do so, one can introduce $\rho_0(t,x)$ as the mass per unit area of the native tissue at the point $x \in \Omega(t)$ at a time t. Let ρ_0^* denote the mass density of native tissue in the absence of any of the lesion component species. Further, each cellular component is taken as mechanically incompressible with a constant reference mass density ρ_j^*, $j = 1,2,3$, that is, ρ_j^* is the mass per unit area of the jth component if none of other components is present. Thus, $\rho_j(t,x)/\rho_j^*$ are the fraction occupied by the jth component at the point x, where $\rho_j(t,x) := m_j n_j(t,x)$ denotes the mass density of the jth component species, and m_j denotes the corresponding mass per unit cell.

We also define the relative total mass density of the cells $a_f(t,x)$ by $a_f(t,x) := \sum_{j=1}^{3} \rho_j(t,x)/\rho_j^*$ (note that $1 - a_f$ corresponds to the "cell mobility"). As it is shown in [7], the following equality holds true,

$$1 - a_f(t,x) = \frac{1}{\rho_0^*}\rho_0(t,x)\,. \tag{11}$$

The full system of equations reads now for $x \in \Omega(t)$

$$\frac{\partial \rho_1}{\partial t} = \mu_1 \Delta \rho_1 - \chi_{11}^0 \nabla \cdot \left((1-a_f)\frac{\rho_1}{c_1}\nabla c_1\right) - d_1 \rho_1 \rho_3 \tag{12}$$

$$\frac{\partial \rho_2}{\partial t} = \mu_2 \Delta \rho_2 - \chi_{21}^0 \nabla \cdot \left((1-a_f)\frac{\rho_2}{c_1}\nabla c_1\right) + \delta \nabla \cdot \left(\frac{\rho_2}{\rho_3}\nabla \rho_3\right) - d_2 \rho_2 \rho_3 \tag{13}$$

$$\frac{\partial \rho_3}{\partial t} = \mu_3 \Delta \rho_3 + d_1 \rho_1 \rho_3 + d_2 \rho_2 \rho_3 \tag{14}$$

$$\frac{\partial c_1}{\partial t} = \nu_1 \Delta c_1 - \alpha_1 \rho_1 c_1 - \alpha_2 \rho_2 c_1 + \gamma \rho_3\,. \tag{15}$$

The modified boundary conditions are for the inner boundary, $x \in \Gamma(t)$,

$$\frac{\partial \rho_1}{\partial \eta} = -\frac{1}{2}\hat{\beta}_0 (c_1 - c_1^*)(1 - a_f) \qquad \frac{\partial \rho_2}{\partial \eta} = 0 \tag{16}$$

$$\frac{\partial \rho_3}{\partial \eta} = 0 \qquad \frac{\partial c_1}{\partial \eta} = 0\,, \tag{17}$$

and for the outer boundary, $x \in \Gamma_1$,

$$\frac{\partial \rho_1}{\partial \eta} = 0 \qquad \frac{\partial \rho_2}{\partial \eta} = -\hat{\beta}_1 (c_1 - c_1^{**})(1 - a_f) \tag{18}$$

$$\frac{\partial \rho_3}{\partial \eta} = 0 \qquad \frac{\partial c_1}{\partial \eta} = 0\,. \tag{19}$$

The previous initial conditions are applied unchanged to the governing equations.

In order to determine the evolution of the inner boundary $\Gamma(t)$, it is useful to represent it parametrically with a family of curves $\gamma(t,\theta) = (x(t,\theta), y(t,\theta))$ for $0 \le \theta \le 2\pi$. Correspondingly, Γ_1 is represented parametrically with the curve $\gamma_1(\theta) = r_1(\cos(\theta), \sin(\theta))$ and the initial location of the inner intimal boundary $\Gamma_0 = \Gamma(0)$ has the parametric representation $\gamma_0(\theta) = r_0(\cos(\theta), \sin(\theta)) = \gamma(0,\theta)$.

To describe the evolution of the inner moving boundary $\Gamma(t)$, we introduce the speed function $s(t,\theta)$ that describes the curve movement in the direction of outward unit normal vector with respect to $\Gamma(t)$. Note that $s(t,\theta)$ can be either positive or negative depending upon whether the intimal boundary is moving inward or outward.

The velocity of the inner intimal boundary $\Gamma(t)$ is then given by

$$s(t,\theta) \,=\, \mu_1\, \hat{\beta}_0\big(c_1(\gamma(t,\theta),t) - c_1^*\big) + \mu_2 \frac{1 - a_f(\gamma_1(t,\theta),t)}{1 - a_f(\gamma(t,\theta),t)} \frac{r_1}{|\partial_\theta \gamma(t,\theta)|} \hat{\beta}_1\big(c_1(\gamma_1(\theta),t) - c_1^{**}\big)\,, \tag{20}$$

see [7]. Note that (20) prescribes a nonlocal and nonlinear dependence of the speed s on all four unknown functions from the system (12) - (15).

3 Numerical methods

To describe methods how to solve numerically the system of partial differential equations (12) - (15), we introduce a representative scalar equation of the form

$$\frac{\partial \rho}{\partial t} = \mu \Delta \rho - \nabla \cdot \left(\vec{V} \rho\right) + F\,, \tag{21}$$

where $\rho = \rho(t,x)$ is an unknown function to be found. The equation (21) is a convection-diffusion-reaction equation, where the diffusion is characterized by a constant parameter μ, the velocity is given by $\vec{V} = \vec{V}(t,x,\rho)$ and reactions are represented by $F = F(t,x,\rho)$.

Each equation of the system (12) - (15) can be formally viewed in the form (21), for instance, the equation (12) is obtained from (21) by considering

$$\rho = \rho_1\,, \quad \mu = \mu_1\,, \quad \vec{V}(t,x,\rho) = \chi_{11}^0 (1 - a_f) \frac{\nabla c_1(t,x)}{c_1(t,x)}\,, \quad F(t,x,\rho) = -d_1 \rho_1 \rho_3\,. \tag{22}$$

A nonlinear coupling of all four equations in (12) - (15) is realized through corresponding velocities $\vec{V}$ and reaction terms F.

The difficulty of solving the problem on a time-dependent domain $\Omega(t)$ will be resolved by considering a fixed domain D that contains the evolving boundary $\Gamma(t) \subset D$ for the whole time interval of the interest. In such a way, the equation (21) will be discretized on a fixed domain with an "active" and "inactive" part.

The position of $\Gamma(t)$ will be described implicitly using a level set method, see a description later. Any nonzero boundary conditions of the form

$$\vec{N}(\gamma) \cdot \nabla \rho(t,\gamma) = f(t,\gamma,\rho)\,, \quad \gamma \in \Omega(t) \tag{23}$$

will be implemented as a source or sink term that can be formally involved in the definition of F. Here $\vec{N}$ is a unit outward normal vector with respect to $\Omega(t)$. Note that (23) can be used for the computations of diffusive fluxes at the boundary, the convective fluxes have to be defined additionally using some standard (inflow, outflow, or noflow) boundary conditions.

3.1 Finite volume discretizaton

To approximate the partial differential equations of type (21), we choose the so called vertex-centered finite volume method. This method was used successfully for convection-diffusion-reaction systems in [4] using the software toolbox UG [1]. The most important advantages of this method is its simplicity even for unstructured grids and a close relation of the numerical model to the analytical (or "physical") model.

Firstly, some standard triangulation of the domain $D \subset R^2$ is required. The domain is fixed and no fitting of the boundary $\Gamma(t)$ is necessary. In our implementation, the triangulation consists of triangles $T^e \subset D$, $e = 1, 2, \ldots, E$ with the vertices x_i, $i = 1, 2, \ldots, I$. The curved part of the boundary ∂D will be only approximated by each particular triangulation, i.e., $D_h \approx D$, where

$$D_h = \bigcup_{e=1}^{E} T^e$$

and $h = h_E$ is some representative parameter (a "discretization" step) of the triangulation. Of course, each successive refinement of the triangulation must produce a more accurate approximation of D.

Having the triangulation, we approximate the analytical function ρ for each discrete time t^n, $n = 0, 1, \ldots$ by a set of nodal values $\rho_i^n \approx \rho(t^n, x_i)$. The values $\rho_i^0 = \rho(0, x_i)$, $i = 1, 2, \ldots, I$ are given by initial conditions.

Having the triangulation and the nodal values, a piecewise linear interpolation $\rho^n(x)$, well-known from standard finite element methods, can be used, and, consequently, a constant gradient $\nabla\rho^n(x)$ for $x \in T^e$ can be computed.

The basic idea of finite volume methods is to integrate the differential equation (21) over a time interval (t^n, t^{n+1}) and a finite volume $\Omega_i \subset D_h$ to obtain

$$\int_{\Omega_i} \left(\rho(t^{n+1}, x) - \rho(t^n, x)\right) dx = \int_{t^n}^{t^{n+1}} \int_{\partial\Omega_i} \vec{N} \cdot \left(\mu\nabla\rho - \vec{V}\rho\right) d\gamma dt + \int_{t^n}^{t^{n+1}} \int_{\Omega_i} F \, dx dt \,, \tag{24}$$

where $\vec{N} = \vec{N}(\gamma)$ is a normal unit vector at $\gamma \in \partial\Omega_i$ pointing outward with respect to Ω_i.

The vertex-centered finite volumes Ω_i will be associated with the nodes x_i by constructing a dual mesh with respect to the primal mesh of triangles. The basic idea is to create polygonal boundaries $\partial\Omega_i \cap T^e$ by connecting the midpoints of edges with the barycenters of triangles T^e. For $x_i \in \partial D$, the boundary $\partial\Omega_i$ contains corresponding halves of edges lying on the boundary ∂D_h, see Figure 2 for an illustration or [3] for more details. Moreover, the following notations will be used for $i = 1, \ldots, I$, $j = 0, \ldots, I$, and $e = 1, \ldots, E$,

$$\Gamma_{i0}^e := \partial\Omega_i \cap \partial D_h \cap T^e \,, \quad \Gamma_{ij}^e := \partial\Omega_i \cap \partial\Omega_j \cap T^e \quad \Rightarrow \quad \partial\Omega_i = \bigcup_e \bigcup_j \Gamma_{ij}^e \,. \tag{25}$$

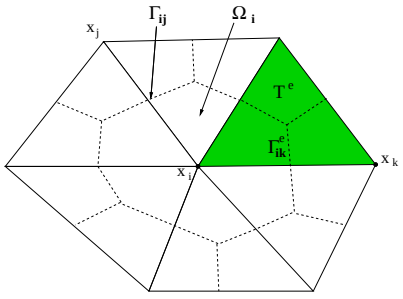

Figure 2: The dual finite volume mesh constructed with respect to primal triangular mesh.

Applying some basic numerical integration rules to (24), one obtains the discrete scheme

$$|\Omega_i| \left(\rho_i^{n+1} - \rho_i^n\right) - \Delta t^n \sum_e \sum_j |\Gamma_{ij}^e| \vec{N}(\gamma_{ij}^e) \cdot \left(\mu \nabla \rho - \vec{V} \rho\right) (t^{n+1}, \gamma_{ij}^e) = \Delta t^n |\Omega_i| F_i^{n+1}, \tag{26}$$

where $(\cdot)\,(t^{n+1}, \gamma_{ij}^e)$ means the evaluation of functions in parentheses $(\cdot)$ for $t = t^{n+1}$ and $x = \gamma_{ij}^e$ with $\gamma_{ij}^e \in \Gamma_{ij}^e$ being an integration point, e.g., the middle point of Γ_{ij}^e. Finally, $F_i^{n+1} := F(t^{n+1}, x_i, \rho_i^{n+1})$.

The boundary conditions (23) for $\gamma \in \partial D$ can be naturally included in the discrete scheme (26) by using (23) evaluated at (t^{n+1}, γ_{i0}^e) to replace the diffusive flux at boundary for (t^{n+1}, γ_{i0}^e). Analogously, the discrete convective flux $\vec{N} \cdot \vec{V} \rho$ must be replaced using some standard boundary conditions.

Note that if discrete equations (26) are derived for the system (12) - (15), they form a fully coupled nonlinear algebraic system that must be solved by some iterative method.

The time discretization used in (26) can be viewed as the implicit Euler (backward) method. The so called Crank-Nicholson time discretization, that is formally second order accurate, can be obtained analogously.

3.2 Upwind scheme

Concerning the approximation of convective-diffusive flux, the scheme (26) can be seen as a second order accurate approximation. Unfortunately, for the case of convection-dominated transport it can produce numerical solutions with non-physical oscillations. Moreover, iterative solvers used to solve the resulting algebraic systems can fail in such a case. To avoid these difficulties, the so called partial upwind scheme can be applied.

To introduce such an upwind scheme, the computation of gradients $\nabla \rho^n(x)$ shall be described in more details. If three vertices of T^e are x_{i_0}, x_{i_1} and x_{i_2}, the constant gradient $\nabla \rho^n(x)$ for $x \in T^e$ can be obtained from

$$\nabla \rho^n(x) = (\rho_{i_1}^n - \rho_{i_0}^n) \vec{G}_{i_1 i_0}^e + (\rho_{i_2}^n - \rho_{i_0}^n) \vec{G}_{i_2 i_0}^e \,, \tag{27}$$

where the constant vectors $\vec{G}_{i_1 i_0}^e$ and $\vec{G}_{i_2 i_0}^e$ are obtained using an inverse of the so called Jacobian 2×2 matrix,

$$\vec{G}_{i_1 i_0}^e = \begin{pmatrix} x_{i_1} - x_{i_0} \mid x_{i_2} - x_{i_0} \end{pmatrix}^{-1} \cdot \begin{pmatrix} 1 \\ 0 \end{pmatrix}, \quad \vec{G}_{i_2 i_0}^e = \begin{pmatrix} x_{i_1} - x_{i_0} \mid x_{i_2} - x_{i_0} \end{pmatrix}^{-1} \cdot \begin{pmatrix} 0 \\ 1 \end{pmatrix}. \tag{28}$$

Following [2], the so called local Peclet numbers $|P|$ can be defined by

$$P = P(t^n, \gamma_{ij}^e) := \frac{1}{\mu} \frac{|\Gamma_{ij}^e| \vec{N}(\gamma_{ij}^e) \cdot \vec{V}(t^n, \gamma_{ij}^e)}{(|\Gamma_{ij}^e| \vec{N}(\gamma_{ij}^e) + |\Gamma_{ik}^e| \vec{N}(\gamma_{ik}^e)) \cdot \vec{G}_{ij}^e} \tag{29}$$

where the index k denotes the third vertex x_k of the triangle T^e additionally to $x_i \in T^e$ and $x_j \in T^e$. The value $\rho(t^{n+1}, \gamma_{ij}^e)$ in the convective flux $\vec{V} \rho$ of (26) can now be approximated by the value $\rho_{ij}^{e,n+1}$, i.e.,

$$\rho_{ij}^{e,n+1} = \begin{cases} -\frac{1}{P} \rho_i^{n+1} + (1 + \frac{1}{P}) \rho_j^{n+1} & P < -2 \\ 0.5 (\rho_i^{n+1} + \rho_j^{n+1}) & -2 \le P \le 2 \\ (1 - \frac{1}{P}) \rho_i^{n+1} + \frac{1}{P} \rho_j^{n+1} & P > 2 \,. \end{cases} \tag{30}$$

Replacing the values $\rho(t^{n+1}, \gamma_{ij}^e)$ in (26) by $\rho_{ij}^{e,n+1}$, a more stable discretization scheme is obtained. In fact, it is useful to compute each example on a chosen grid with and without using the upwind method (if possible) and to compare obtained numerical results.

3.3 Approximation of the moving boundary

To describe the features of our model related to the moving boundary $\Gamma(t)$, a numerical level set function with the following properties will be used.

Firstly, for each time level $t = t^n$, a discrete set of nodal values ϕ_i^n will be available. The property $\phi_i^n < 0$ indicates that at $t = t^n$ the node x_i does not belong to $\Omega(t^n)$, and, analogously, if $\phi_i^n > 0$ then $x_i \in \Omega(t^n)$. The case $\phi_i^n = 0$ indicates that $x_i \in \Gamma(t^n)$.

Supposing a standard linear interpolation in space of the nodal values ϕ_i^n and searching for a zero contour line of such an interpolation, a polygonal approximation $\Gamma_h(t^n) \approx \Gamma(t^n)$ can be easily obtained. This approximation has the property that $\Gamma_h(t^n) \cap T^e$ is either an empty set, a corner of T^e, or a line in T^e. Consequently, one can use the notation

$$\Gamma_{i,e}^n := \Gamma_h(t^n) \cap \Omega_i \cap T^e \quad \Rightarrow \quad \Gamma_h(t^n) = \bigcup_i \bigcup_e \Gamma_{i,e}^n \,. \tag{31}$$

The approximative time-dependent domain $\Omega_h(t^n)$ is now defined by its boundaries $\Gamma_h(t^n)$ and ∂D_h.

Now we describe the implementation of the discrete scheme (26) for the approximation of equation (21) with boundary conditions (23) on an implicitly given boundary $\Gamma_h(t^n)$.

Firstly, if $|\Gamma_{i,e}^n| \neq 0$, one has to add the contribution of boundary conditions (23) defined on $\Gamma_{i,e}^n$ to the i-th discrete equation in (26). This can be realized formally by redefining F_i^{n+1} in (26) taking

$$F_i^{n+1} = F(t^{n+1}, x_i, \rho_i^{n+1}) + \frac{1}{|\Omega_i|} \sum_e |\Gamma_{i,e}^n| \mu f(t^{n+1}, \gamma_{i,e}^n, \rho^{n+1}(\gamma_{i,e}^n)) \,, \tag{32}$$

where $\gamma_{i,e}^n \in \Gamma_{i,e}^n$ is an integration point, e.g., the middle point of the line $\Gamma_{i,e}^n$. An analogous treatment is necessary for discrete convective fluxes.

Next, we describe how the discrete scheme (26) shall be treated if $\phi_i^n < 0$ or $\phi_j^n < 0$ for at least one index i or j occurring in (26). The simplest variant is to require that $\mu \equiv 0$ and $\vec{V} \equiv \vec{0}$ for each triangle T^e such that one has $\phi_{i_j}^n < 0$ for all three corners x_{i_j}. This means that no diffusive-convective flux is allowed in T^e that lies completely in the inactive part of D_h. Consequently, if this is true for all triangles T^e such that $x_i \in T^e$, the discrete equation (26) takes the trivial form $\rho_i^{n+1} = \rho_i^n$.

On the other hand, if one has $\phi_j^n > 0$ for at least one corner x_{i_j}, a standard approximation for the diffusive-convective flux can be used as defined in (26). This means that the i-th discrete equation can adopt some "non-trivial" form even for nodes x_i that lies outside of $\Omega_h(t^n)$, but there exists at least one neighbour x_j such that $x_j \in \Omega_h(t^n)$.

Note that in our numerical scheme (26), the finite volumes Ω_i are always fixed. Therefore, the (approximative) mass in $\Omega_h(t^n)$, if necessary, shall be computed by $\sum_i |\Omega_i \cap \Omega_h(t^n)| \rho_i^n$.

4 Level set method

Finally, we describe briefly how the numerical level set function can be obtained. The speed $s(t, \gamma)$ of the evolution of $\Gamma(t)$ from (20) can be used to define the advective level set equation

$$\frac{\partial \phi(t,x)}{\partial t} + s(t,x) |\nabla \phi(t,x)| = 0 \,, \tag{33}$$

see standard reference books [11, 10] on this topic. Analogously, several level set methods to find an approximative solution of (33) can be found there, or a finite volume discretization closely related to vertex-centered finite volume meshes can be found in [9]. Note that the equation (33) shall be solved on D, and, consequently, the velocity s must be formally defined on (or extended to) the whole domain D.

We implement the so called "flux-based" level set method, see [5], in which the equation (33) is formally redefined to

$$\frac{\partial \phi}{\partial t} + \nabla \cdot \left(\vec{Q} \phi \right) = \phi \nabla \cdot \vec{Q} \,, \tag{34}$$

where $\vec{Q} = s \nabla \phi / |\nabla \phi|$. The discrete scheme then takes the form [5]

$$|\Omega_i| \left(\phi_i^{n+1} - \phi_i^n \right) + \Delta t^n \sum_e \sum_j |\Gamma_{ij}^e| \min\{0, \vec{N}(\gamma_{ij}^e) \cdot \vec{Q}(t^n, \gamma_{ij}^e)\} (\phi_i^n - \phi_j^n) = 0 \,. \tag{35}$$

The dependence of $\vec{Q}$ on $\nabla \phi(t^n, \gamma_{ij}^e)$ for $\gamma_{ij}^e \in T^e$ is resolved by computing the gradient of ϕ using the standard linear interpolation of nodal values ϕ_i^n for vertices x_i of a triangle T^e.

The scheme (35) is formally a first order accurate approximation of the level set equation (33), a second order accurate form can be found in [6].

5 Numerical results

The current section is intended to show some preliminary numerical results and to demonstrate some behavior of the numerical solutions that is expected by the system governed by (12) - (15). For the numerical investigations we use the software toolbox UG [1]. For all numerical simulations the initial conditions and boundary conditions are given by (16) - (19) and the parameter values are listed in Table 1 (also given in [8]). The function a_f is computed by $a_f = \sum_{j=1}^{3} \rho_j$, that is, $\rho_j^* \equiv 1$, $j = 1, 2, 3$, for all numerical computations.

μ_1	0.005	χ_{11}^0	3.0	d_1	1.0	δ	0.01
μ_2	0.005	χ_{21}^0	3.0	d_2	0.01	α_1	0.1
μ_3	0.005	ν_1	0.1	γ	30	α_2	0.05
β_1	$0.1\mu_1$	β_2	$0.1\mu_2$	c_1^*	0.1	c_1^{**}	0.1
		c_1^0	0.1	ϵ_3	0.01	Q_3	25

Table 1: Parameter values

We remark that the initial conditions can be interpreted as follows: At the interface between the lumen and the intima, there is a small radially symmetric concentration of immune cells. We seed the intima with a small concentration of debris at some arbitrarily fixed point x ($x = (0.8, 0)$) within the intima. Furthermore, we assume a small uniform distribution of chemoattractants. The initial condition on the smooth muscle cells is similar to the initial condition on the immune cells and corresponds to a small axisymmetric concentration of smooth muscle cells (SMCs) on the outer boundary where the intima meets the media. The boundary condition on this outer boundary reflects the migration–positive chemotaxis of SMCs from the media as discussed in Section 2.3 and 3.2 of Ibragimov et al. [8].

Figure 3 shows an initial evolution of all species for this example (after a second time step). Further temporal behavior of the concentrations can be seen from Fig. 4 and Fig. 5.

There, one can observe time evolution of the concentration of immune cells from an axisymmetric initial distribution to a highly localized dense accumulation near the point which was seeded with a small amount of debris at time zero. Similarly, the SMCs enter into the region of the lesion through the outer boundary corresponding to the media. The temporal evolution given by the numerical results also shows that the artery wall dilates first, and, eventually, the lesion bulges into the lumen.

One of the primary interests in the final numerical solutions is a situation when there is a region of lower density of SMCs. Such a situation can correspond to points of the highest concentration of immune cells, i.e., to the cap intended to isolate the lesion. An evidence of such a cap formation, as described in [8], is of great interest.

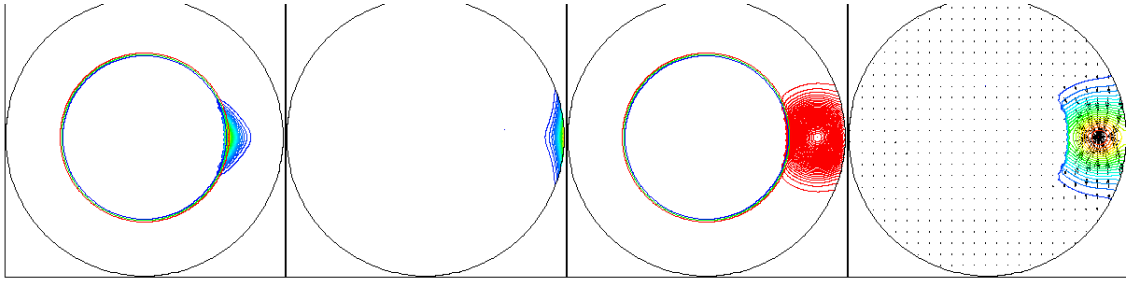

Figure 3: Concentration plots after two time steps. From left to right: ρ_1, ρ_2, ρ_3, and c_1. Additionally, the contours of the level set function are shown in the first and third plot, and the velocity $\nabla c_1/c_1$ is shown in the fourth plot.

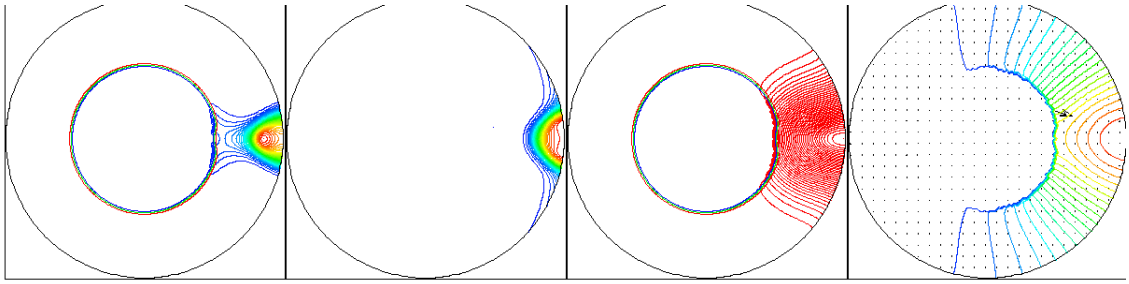

Figure 4: Concentration plots after 100 time steps, for a description see Figure 3.

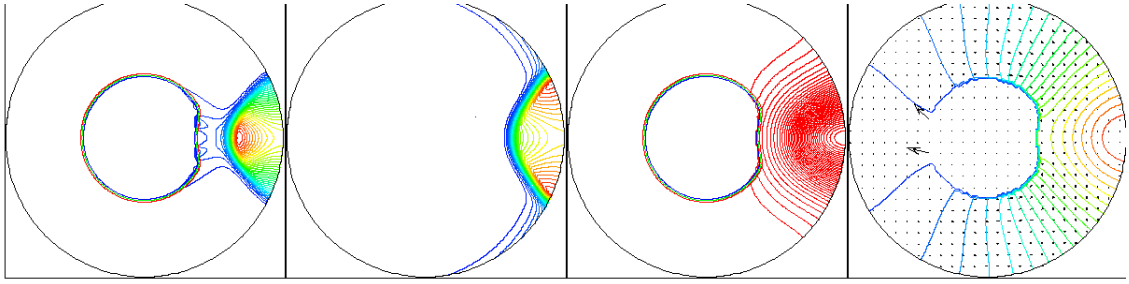

Figure 5: Concentration plots after 200 time steps, for a description see Figure 3.

Finally, Figure 6 and Figure 7 show the maximal concentration for different cell species and chemoattractants as functions of time. As it is shown in Figure 7, the concentration of debris firstly decreases before it starts to grow later. This shows clearly that the healing impact of the immune cells and the SMCs is too weak.

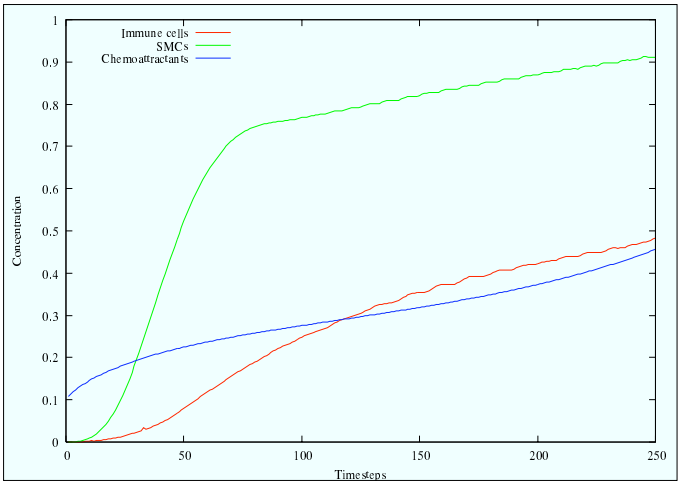

Figure 6: Maximal concentration of the immune cells ρ_1, smooth muscle cells ρ_2, and the chemoattractants c_1 as a function of time.

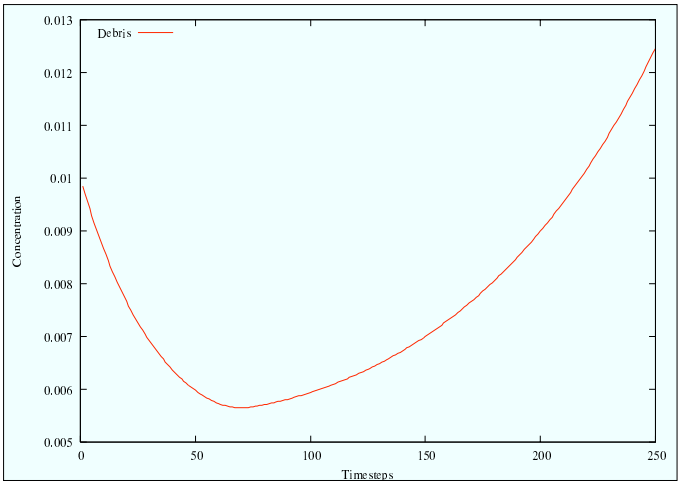

Figure 7: Maximal concentration of the debris ρ_3 as a function of time.

Note that the presented example was chosen only to check if described numerical methods are capable of solving the mathematical model and if an expected qualitative behavior of numerical solutions can be confirmed. Both aspects of numerical methods were confirmed for this example, nevertheless, further significant improvements are planned for the future that will be reported elsewhere.

6 Summary

In this paper we consider a free boundary problem modeling the growth of an atherosclerotic lesion. We perform numerical simulations using fully implicit finite volume discretization method. The moving boundary problem is solved within the framework of a level set formulation that enables an application of fixed grids. Analogously to previous numerical studies [8], the simulations demonstrate that our numerical model captures certain observed features such as the localization of immune cells, the build-up of lipids and debris, and the isolation of a lesion by smooth muscle cells. Additionally, the numerical simulations exhibit that the artery wall is remodeled by dilating and that, eventually, the lesion bulges into the lumen causing some degree of occlusion of the artery.

References

[1] P. Bastian, K. Birken, K. Eckstein, K. Johannsen, S. Lang, N. Neuss, and H. Rentz-Reichert. UG — a flexible software toolbox for solving partial differential equations. *Computing and Visualization in Science*, 1(1):27–40, 1997.

[2] P. Frolkovič. Maximum principle and local mass balance for numerical solutions of transport equation coupled with variable density flow. *Acta Mathematica Universitatis Comenianae*, 67(1):137–157, 1998.

[3] P. Frolkovič. Discretization. In E. Fein, editor, *D^3F - ein Programmpaket zur Modellierung von Dichteströmungen*, Braunschweig, 1999. GRS-139, ISBN 3-923875-97-5, (see also http://sit.uni-hd.de).

[4] P. Frolkovič. The simulator and the methods used. In E. Fein, editor, *R^3T - A program suite to model transport and retention in porous media*, GRS-192, ISBN-3-391995-60-7, Braunschweig, 2003.

[5] P. Frolkovič and K. Mikula. Flux-based level set method: A finite volume method for evolving interfaces. Preprint 15, Interdisziplinäres Zentrum für Wissenschaftliches Rechnen, September 2003.

[6] P. Frolkovič and K. Mikula. High-resolution flux-based level set method. Technical Report 12, Department of Mathematics and Descriptive Geometry, Slovak University of Technology, 2005.

[7] A. I. Ibragimov, C. J. McNeal, L. R. Ritter, and J. R. Walton. A free boundary problem modeling growth of an atherosclerotic lesion. Preprint, Texas A&M University, College Station, TX, 2005.

[8] A. I. Ibragimov, C. J. McNeal, L. R. Ritter, and J. R. Walton. A mathematical model of atherogenesis as an inflammatory response. *Mathematical Medicine and Biology*, 22(4):305–333, 2005.

[9] G. Kossioris, Ch. Makridakis, and P.E. Souganidis. Finite volume schemes for Hamilton-Jacobi equations. *Numer. Math.*, 83:427–442, 1999.

[10] S. Osher and R. Fedkiw. *Level Set Methods and Dynamic Implicit Surfaces.* Springer, 2003.

[11] J. Sethian. *Level Set Methods and Fast Marching Methods.* Cambridge University Press, 1999.